

Optimizing and using AI to study of the cross-section of finned tubes for nanofluid-conveying in solar panel cooling with phase change materials

Chaoyang Zhu

Institute of Social Innovation and Public Culture, Communication University of China Beijing, 100024, China



ARTICLE INFO

Keywords:
 Thermal solar panel
 Square pipe
 Elliptical pipe
 Circular pipe
 Nanofluid
 Meshless

ABSTRACT

This study numerically investigated the effect of applying different shapes of nanofluid-conveying pipes on a thermal solar panel system. Two pipes with circular, elliptical, and square shapes were employed in this system. Likewise, paraffin wax Phase Change Material (PCM) was used in the solar thermal panel. A large number of spherical pin fins were installed over the pipes inside the PCM. The two phases of the NF were simulated, and all equations were solved using an element-free Galerkin method based on weak form. The results showed that the elliptical pipes increased the volume of the liquid PCM around them, while the circular pipes raised the quantity of solid PCM around them. That is to say, these two pipe types brought about the maximum difference in the volume of the phase change material (5%). When $t = 2000$ s, the temperature could decrease by >1% through circular rather than elliptical pipes. In the same period, the heat transfer rate of the circular pipes was 16.17% above that of elliptical pipes, whose heat transfer was 48.43% higher compared to the square pipes. When the solar panel was hot, elliptical pipes maximized the temperature of the output NF, and circular pipes minimized the NF's temperature at the outlet.

1. Introduction

The sun is the most widespread source of energy in the globe. The optical energy radiated from the sun to the earth per hour exceeds the total energy the earth's inhabitants consume in a year. However, the density of this energy is too low despite its extensiveness. The sun is not only a fantastic energy source, but also the source of all other energies and the place where life first began [1]. Solar energy is also a source of fossil energy since fossil fuels were once plants whose life depended on the sun. To benefit from this source, we should look for an approach to convert its scattered energy into consumable electric energy with high efficiency and low cost [2]. Humans have long exploited solar energy using various methods. Today, with technological developments, humans take steps to exploit solar energy as much as possible [3–5]. The utilization of various solar collectors for generating warm water is an instance of using solar energy. Different types of solar collectors can generate warm water and even electricity at various temperatures [6–8]. Flat-plate collectors are among the most prevalent types of solar collectors that have been extended due to their simple fabrication [9–11]. Today, an approach to meeting energy needs is to utilize photovoltaic systems to convert solar energy to electric energy [12–14]. A tiny percentage of the absorbed radiant energy is converted to electric energy by

photovoltaic cells, while a large portion is transformed into thermal energy and increases the temperature of the cells. The most important part of a photovoltaic system are the PV cells, and when the temperature of the cells increases, the efficiency of the system decreases [15,16]. Hence, the temperature of the PV cells should be decreased as much as possible for the purpose of enhancing the efficiency of these systems. Researchers have developed various cooling systems and reached varying results. The phenomenon that produces electricity from solar energy using no electricity drivers is called the photovoltaic phenomenon, and any mechanism exploiting this phenomenon is called a photovoltaic system [17,18]. Solar photovoltaic or solar energy systems are renewable energy equipment that applies PV modules to convert the sun's light into electricity. The generated electricity can either be stored or directly used [19,20]. Photovoltaic systems are the most intensively-used devices in the new energy domain. In the past, numerous studies have targeted solar panels and attempted to improve the efficiency of these apparatuses. An approach to enhancing the efficiency of solar panels is to combine them with other solar equipment, such as solar collectors, solar stills, etc. In solar panels, it is feasible to generate power in parallel with warming water and raise the total efficiency of the solar system. Krauter et al. [21] investigated the effect of the continuous flow of water over photovoltaic arrays to cool the system

E-mail address: czhu4043@gmail.com.

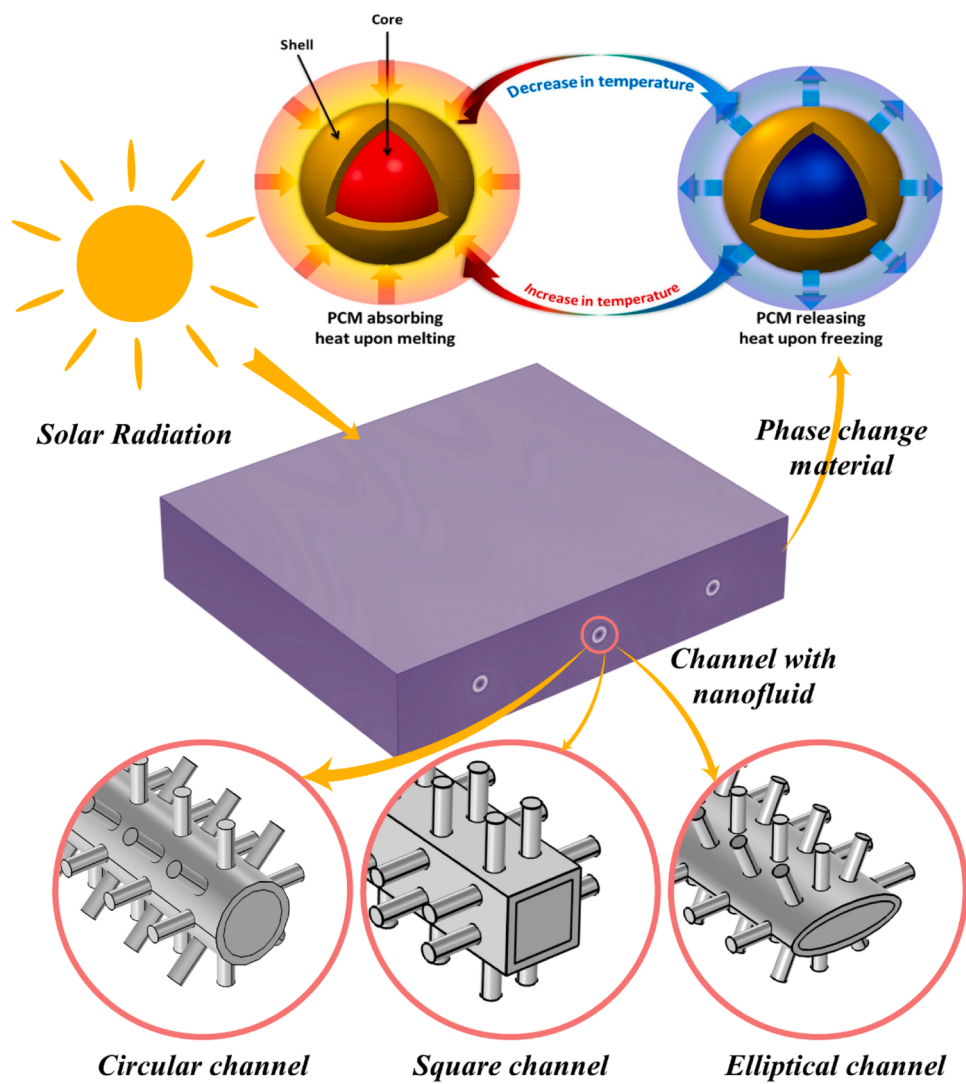


Fig. 1. Schematics of the solar thermal panel with various pipe shapes.

Table 1
Values of properties of nanoparticles, water, and PCM [29].

	Cp(J/kg K)	$\rho(\text{kg/m}^3)$	$\mu(\text{kg/m s})$	k(W/m K)
Ag (diameter=40 nm)	235	10,500	–	429
Water	4179	997.1 melting point (°C)	0.001 k(W/m)	0.613 Heat latent (J/g)
Paraffin wax	27.7	0.365	–	202.1

Table 2
Average temperature values vs. various solar fluxes in the present work and studies by Nasrin et al. [33] and Rahman et al. [34].

Solar irradiance (W/m ²)	397	587	704	852	997
Nasrin et al. [33]	31.4	34.9	39	43.8	47.5
Rahman et al. [34]	32.5	36.5	40.6	45.7	49.4
Present work	31.8	35.4	39.8	44.2	48.1

and reduce reflection losses from the panel surface by measuring power through variable resistors. Hartmann et al. [22] examined the cooling of PV cells and solar collectors in two different European climates (Madrid

and Freiburg). Kim et al. [23] could improve the efficiency of a photovoltaic panel by designing a cooling system in the climatic condition of South Korea. Prudhviand Sai [24] cooled photovoltaic panels and improved their efficiency by applying natural approaches in greenhouses and plant sites. Teo et al. [25] designed a thermal-photovoltaic module and examined it in the presence and absence of a cooling system. They could obtain a linear relationship between the efficiency and temperature of the system. In their experiment, the efficiency of the solar cells was 2–9% in the absence of a cooling system and 12–14% in the presence of a cooling system. By applying a water flow below the panel surface, Habiballahi et al. [26] could improve the efficiency of photovoltaic systems and enhance the total efficiency by 1.08%. At the University of Patras, Tripanagnostopoulos et al. [27] ran an economic analysis on thermal-photovoltaic systems and compared the results with the standards of photovoltaic panels.

Today, solar thermal panels are employed in locations with energy shortages and remote regions to supply the demanded warm water and electricity. Due to the many difficulties these modules bring, the current research employed PCM in the system to imitate a solar thermal panel. As significant elements in solar thermal panels, this study investigated the effect of the pipe shape on the panel temperature, variations in the volume of the phase change material, heat transfer coefficient, and NF temperature. The NF flowing inside the pipes was simulated in two phases. The analysis was transient and 3-dimensional and targeted the

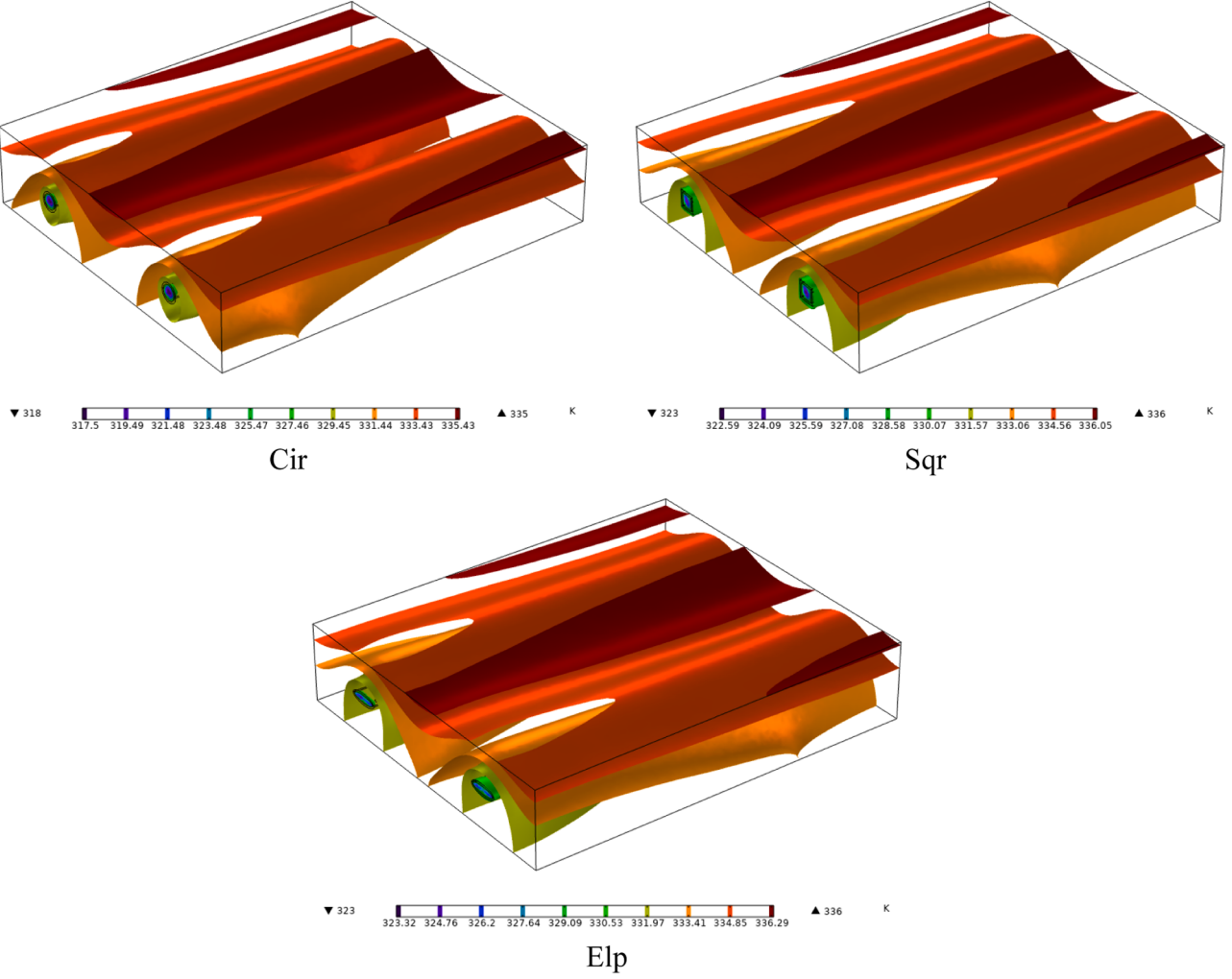


Fig. 2. The isothermal plates on the solar panel and PCM for three shapes of pipes at the final time.

PCM melting and temperature contours.

2. Definition of the problem

As Fig. 1 illustrates, the examined solar panel below which two pipes are laid has 1000 mm × 850 mm dimensions. The pipes are located in a 200 mm-thick layer of paraffin wax PCM that is used as the panel's substructure. Spherical pin fins with a 25 mm height and 10 mm diameter are used over the pipes. The effect of three shapes of pipes, i.e., circular (Cir), elliptical (Elp), and (Sqr), conveying the water NF and silver nanoparticles, is examined at the inlet temperature of 298 K. The diameter of the circular pipe equals 50 mm, and the elliptical pipe has a short diameter of 5.5 mm and a long diameter of 115 mm. Every side of the square pipes equals 43.3 mm, and the thickness of the pipes is 10 mm.

Table 1 presents the values of the properties of the nanoparticles, water, and PCM [28].

3. Governing equations

In the following, the equations of the NF in the laminar flow and Newtonian fluid states for the conservation of mass, momentum, energy, and volume fraction are presented [30].

$$\nabla \cdot (\rho_m \vec{v}_m) = 0 \quad (1)$$

$$\nabla \cdot (\rho_m \vec{v}_m \vec{v}_m) = -\nabla p + \nabla \cdot (\mu_m \nabla \vec{v}_m) + \nabla \cdot \left(\sum_{k=1}^n \varphi_k \rho_k \vec{v}_{dr,k} \vec{v}_{dr,k} \right) \quad (2)$$

$$\nabla \cdot \left(\sum_{k=1}^n \varphi_k \vec{v}_k (\rho_k H_k + P) \right) = \nabla \cdot (k_m \nabla T) \quad (3)$$

$$\nabla \cdot (\varphi_p \rho_p \vec{v}_m) = \nabla \cdot (\varphi_p \rho_p \vec{v}_{dr,p}) \quad (4)$$

The equations for \vec{v}_m , $\vec{v}_{dr,k}$, and \vec{v}_{pf} are provided below.

$$\vec{v}_m = \frac{\sum_{k=1}^2 \phi_k \rho_k \vec{v}_k}{\rho_m} \quad (5)$$

$$\vec{v}_{dr,k} = \vec{v}_k - \vec{v}_m \quad (6)$$

$$\vec{v}_{pf} = \vec{v}_p - \vec{v}_f \quad (7)$$

In the following, the equations for the relationships between \vec{v}_{pf} and $\vec{v}_{dr,p}$, and \vec{v}_{pf} and f_{drag} are presented [31,32].

$$\vec{v}_{dr,p} = \vec{v}_{pf} - \sum_{k=1}^n \frac{\varphi_k \rho_k}{\rho_m} \vec{v}_k \quad (8)$$

$$\vec{v}_{pf} = \frac{\rho_p d_p^2}{18 \mu_c f_d} \frac{(\rho_p - \rho_m)}{\rho_p} \left[\vec{g} - (\vec{v}_m \cdot \nabla) \vec{v}_m \right] \quad (9)$$

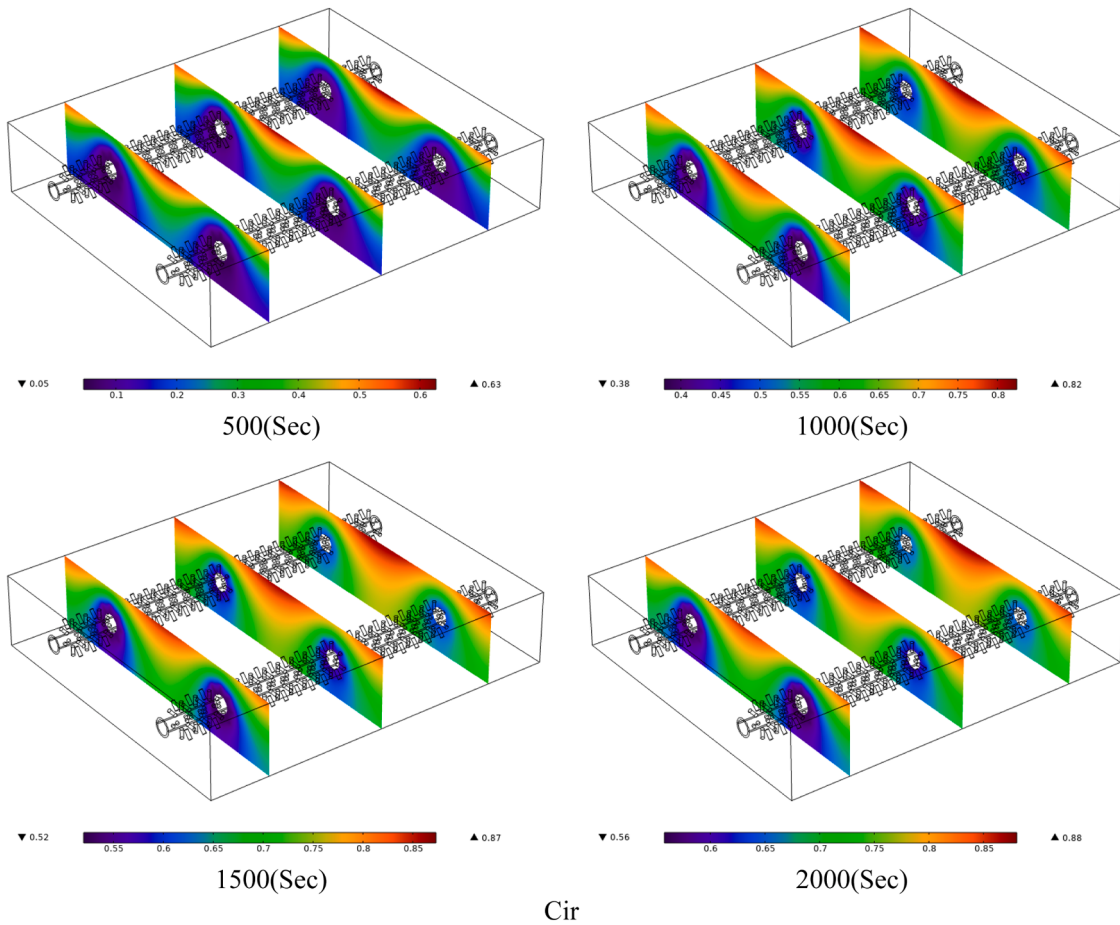


Fig. 3. The contour of the molten PCM in three vertical sections vs. four different times for three pipe shapes.

$$f_{drag} = \begin{cases} 1 + 0.15 Re_p^{0.687} Re_p \leq 1000 \\ 0.0183 Re_p Re_p > 1000 \end{cases} \quad (10)$$

Three phases occur during the heating or cooling of per PCM element. For example, in the first phase, the temperature of the solid PCM element rises to reach the melting point. In the second phase, the element is heated at a constant temperature as much as its latent heat is multiplied by its mass. Finally, when the element is melted, the temperature of the liquid PCM element goes up. Thus, the PCM enthalpy consists of three phases:

$$H_{solidphase} \leq C_s(T_m - T_{ref}) \text{ IF } T_p < T_m \quad (11)$$

$$H_{liquidphase} > C_s(T_m - T_{ref}) + H_L \text{ IF } T_p > T_m \quad (12)$$

$$C_s(T_m - T_{ref}) < H_{meltingduration} < C_l(T_m - T_{ref}) + H_L \text{ IF } T_p = T_m \quad (13)$$

$$H_{solidphase} = C_s(T_p - T_{ref}) \quad (14)$$

$$H_{liquidphase} = C_l(T_p - T_m) + H_L + C_s(T_m - T_{ref}) \quad (15)$$

Hence, we can write T_p , i.e., the enthalpy-based PCM temperature, as below:

$$T = \begin{cases} T_{ref} + \frac{H}{C_s} & \text{if } H \leq T_{ref} - T_{ref} \\ T_m & \text{if } C_s(T_m - T_{ref}) < H < C_s(T_m - T_{ref}) + H_L \\ T_m + \frac{H - H_L - C_s(T_m - T_{ref})}{C_l} & \text{if } H \geq C_s(T_m - T_{ref}) + H_L \end{cases} \quad (16)$$

Where T_{ref} indicates the temperature that is equal to or below T_m . As Eq. (16) displays, the T-H relationship is determined with regard to the PCM phase, and a related equation is employed in various conditions. This section examines the generalized enthalpy method, which eliminates the drawbacks of the enthalpy method. This method is first used to obtain the PCM-governing heat transfer equation and then rewrite fluid-governing heat transfer equations in order to standardize the relations. If you look at Eq. (16), you can see that if T_{ref} equals T_m , the enthalpy values will not experience problems versus each other. That is to say, the enthalpy of the solid PCM is negative and zeros when the temperature of the solid PCM reaches the melting point. When the PCM starts melting, its enthalpy is added till it maintains its melting temperature, i.e., when the solid PCM element changes into a liquid state, the specific enthalpy of the PCM increases from zero to H_L , and when the respective element is melted completely, its enthalpy hikes due to the temperature rise.

$$T' = T - T_m \quad (17)$$

Thus, Eqs. (3)–(27) take the following forms:

$$\frac{\partial}{\partial t} (\rho_p H_p) = \frac{\partial}{\partial x} \left(k_p \frac{\partial T'}{\partial x} \right) \quad (18)$$

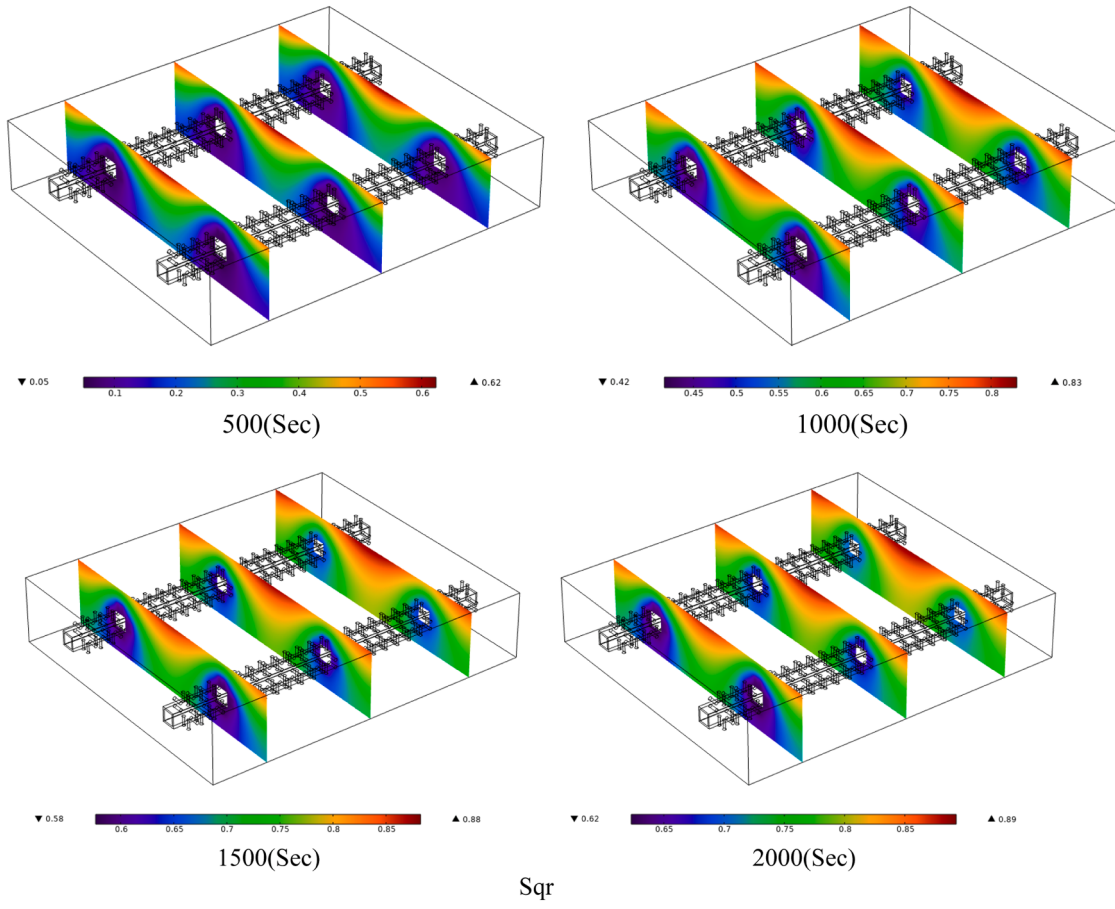


Fig. 3. (continued).

Concerning the definition of the T' , we can explain it as the below equation:

$$T' = \begin{cases} T_m - T & T < T_m \\ 0 & T = T_m \\ T - T_m & T > T_m \end{cases} \quad (19)$$

Notably, when $T = T_m$; then, $T' = 0$. Thus, the PCM enthalpy is explained according to T' :

$$\begin{aligned} H_{\text{solidphase}} &= C_s T' \text{ IF } T' < 0 \\ 0 \leq H_{\text{meltingduration}} &< H_L \text{ IF } T' = 0 \\ H_{\text{liquidphase}} &= H_L + C_s T' \text{ IF } T' > 0 \end{aligned} \quad (20)$$

In other words, T' is explained as the below equation based on the enthalpy:

$$T' = \begin{cases} \frac{H}{C_s} & H \leq 0 \\ 0 & 0 < H < H_L \\ \frac{H - H_L}{C_L} & H \geq H_L \end{cases} \quad (21)$$

It is worth noting that the purpose is to develop the $T = T(H)$ function.

Hence, according to the above equations, we can explain T' as below:

$$T' = A^*(H)H + B^*(H) \quad (22)$$

Where B^* and A^* are the functions of H and are definable as below:

$$A^*(H) = \begin{cases} \frac{1}{C_s} H \leq 0 \\ 0 & 0 < H < H_L \\ \frac{1}{C_L} H \geq H_L \end{cases} \quad (23)$$

$$B^*(H) = \begin{cases} 0 & H \leq 0 \\ 0 & 0 < H < H_L \\ \frac{-H_L}{C_L} & H \geq H_L \end{cases} \quad (24)$$

Now, by considering the obtained relation and substituting it in the equation, we can rewrite the heat transfer-governing equation as below:

$$\frac{\partial}{\partial t} (\rho_p H_p) = \frac{\partial}{\partial x} \left(k_p \frac{\partial A^* H_p}{\partial x} \right) + P \quad (25)$$

Which is written below:

$$P = \frac{\partial}{\partial x} \left(k_p \frac{\partial B^*}{\partial x} \right) \quad (26)$$

Where B^* and A^* are the functions of H and are explained by Eqs. (23) and (24). As observed in Eqs. (25) and (26), the PCM-governing heat transfer equation has changed into a relation in which H is the mere dependent variable and, conversely, has been omitted from the equation. The problem described above was algebraized using the numerical finite element technique, and the equations were then solved using the COMSOL program. This software was also employed for geometry drawing, meshing, and output extraction. Finally, the following relations have been used to obtain the thermal conductivity and viscosity

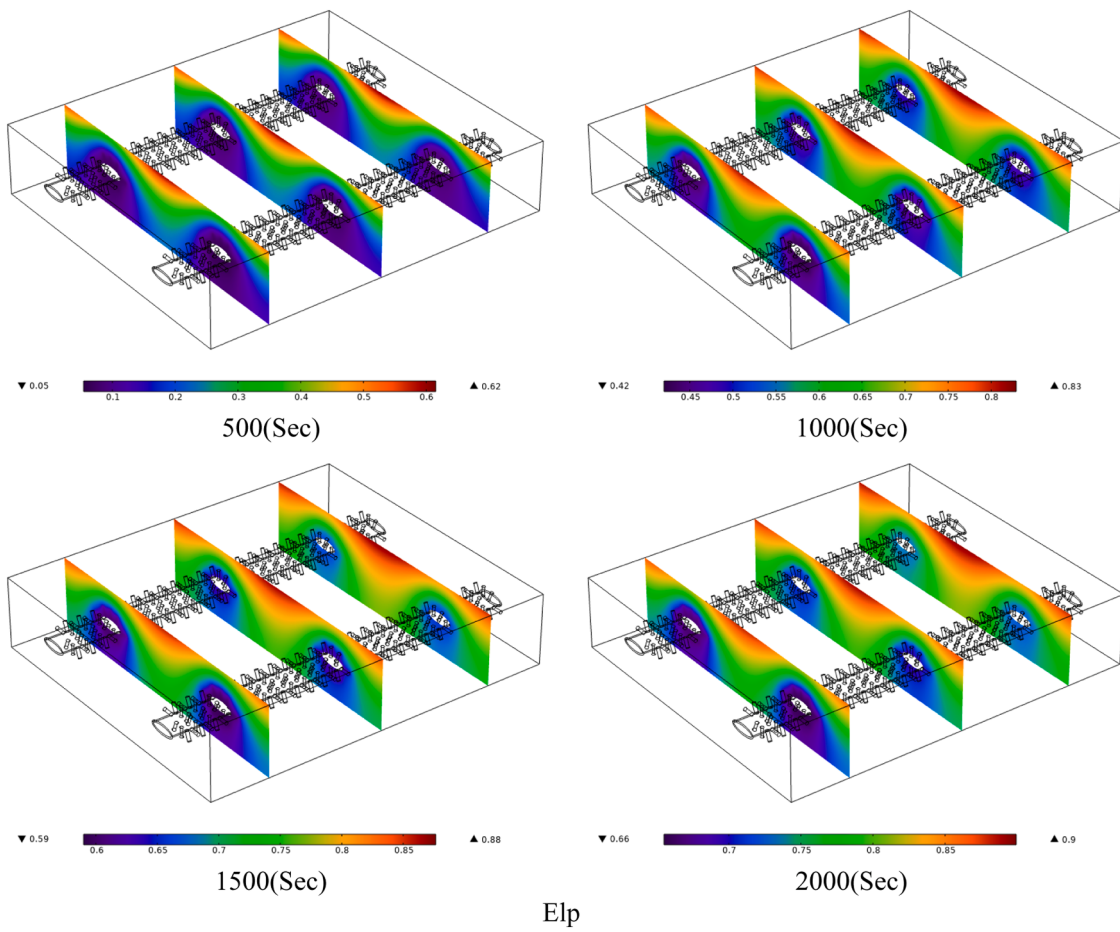


Fig. 3. (continued).

of the nanofluid

$$\frac{\mu_{nf}}{\mu_f} = 1 - 2.5\varphi \quad (27)$$

$$\frac{k_{nf}}{k_f} = 0.981 + 0.00114 \times T + 30.661 \times \varphi \quad (28)$$

3.1. Numerical method, optimization and artificial intelligence

Simulations are conducted in the software environment of COMSOL Multi-physics using the finite element method. COMSOL is suitable for interdisciplinary research because of being all-purpose. Although there are other multi-physics software programs, COMSOL's strength lies in its ability to model systems whose governing equations come from completely unrelated fields more quickly and simply. The default modules for system simulation and analysis are the cause of this. For the simulation and analysis of PCM, COMSOL has a dedicated module. The coupling of this module with heat transfer and flow under the panel is one of the significant and useful sub-branches. Other governing equations' presumptions are also applied in the software environment for simulation along with the 3D modeling software. Some simplifications are necessary for solving Navier-Stokes equations in order to reduce the number of computational resources needed, as all solvers of simplified Navier-Stokes equations need a lot of processing time and memory.

To solve this issue, the finite element method is used. The majority of physics and engineering problems whose governing behavior can be expressed by a system of differential equations can be roughly solved numerically using the finite element method. A collection of statistical techniques known as the response surface methodology (RSM) are

applied in the optimization of procedures where some variables affect the desired response. The mathematical model's graphical schematic provides the RSM definition. With this statistical approach, fewer experiments are required to estimate all quadratic regression model coefficients as well as the interdependencies between various factors. The statistical response surface scheme is chosen because the primary challenge of this study is to examine the primary and reciprocal effects of factors. The effects of independent variables are evaluated in this study at three different levels, according to a recent equation. In this equation, \bar{X}_i stands for the dimensionless value of the process independent variable, \bar{X}_i for the variable's actual value, \bar{X}_i for its actual value at the central point, and ΔX_i for the step change. In the second step, the statistical design is selected, the relationship used for prediction is fitted and evaluated. RSM typically employs a quadratic equation as its model. For each independent variable in RSM, a model is defined that expresses the primary and reciprocal effects of factors on each variable separately. The following gives a presentation of the multi-variable model. In this model, Y is the predicted response, β_0 is a constant coefficient, β_1 , β_2 , and β_3 are the linear effects, β_{11} , β_{22} , and β_{33} are the quadratic effects, and β_{12} , β_{13} , and β_{23} are the mutual effects. The Design Expert software is used for analysis of information and plotting the desired diagrams using RSM.

$$Y = \beta_0 + \beta_1 x_1 + \beta_2 x_2 + \beta_3 x_3 + \beta_{11} x_1^2 + \beta_{22} x_2^2 + \beta_{33} x_3^2 + \beta_{12} x_1 x_2 + \beta_{13} x_1 x_3 + \beta_{23} x_2 x_3 \quad (29)$$

This study utilizes the central composite design with three variables, including temperature, water-to-seed ratio, extraction time, three levels, three blocks, and six iterations in the central design point (for calculating the process repeatability), for examining the effect of inulin

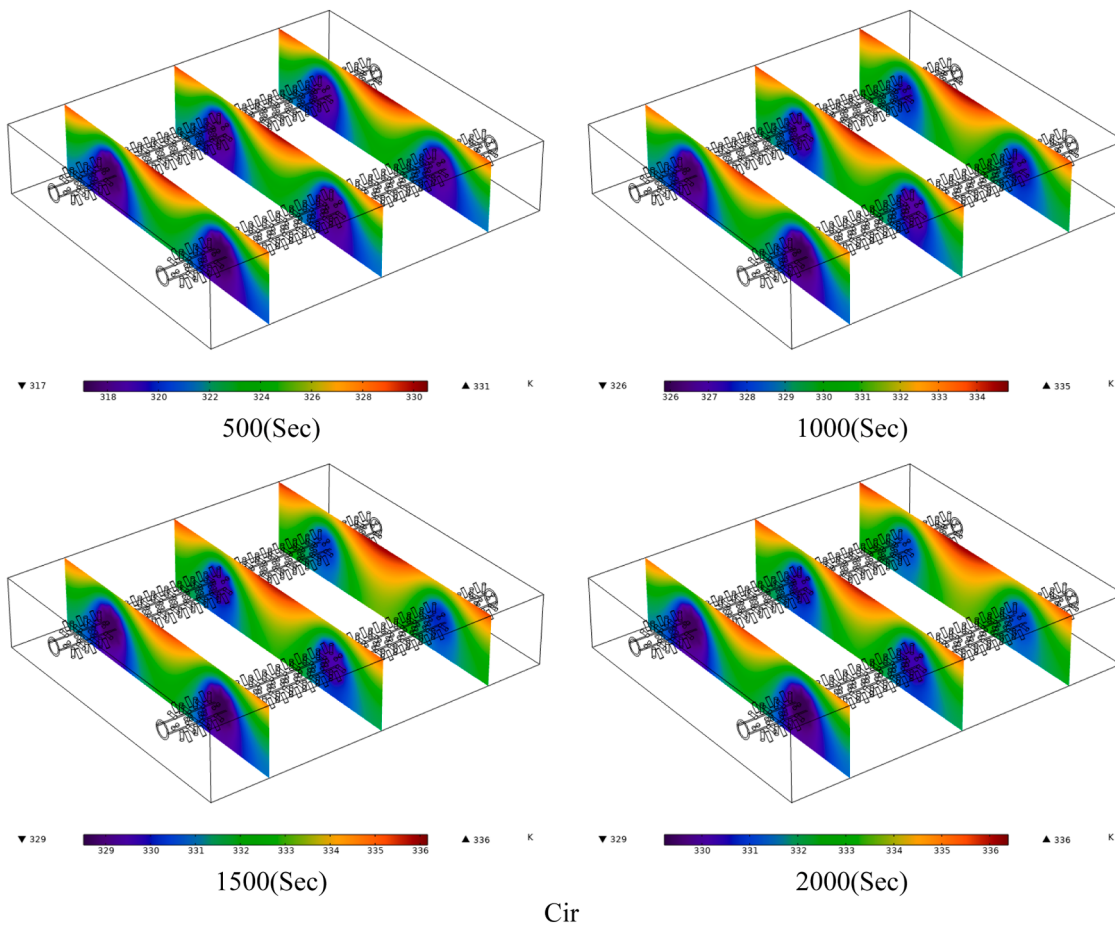


Fig. 4. The temperature contour on three vertical sections of the solar thermal panel and the underlying PCM vs. four different times for circular, elliptical, and square pipes.

extraction and process optimization.

3.2. Validation

The outputs of the current numerical investigation were compared with the findings of experimental works by Nasrin et al. [33] and Rahman et al. [34] for the aim of validation. Table 2 compares the average temperature values of the solar panel in various solar fluxes in the present study and the works by Nasrin et al. [33] and Rahman et al. [34]. As observed, there are trivial differences in the results.

4. Results and discussion

Fig. 2 displays isothermal plates on the solar panel and PCM for three shapes of pipes, i.e., circular, elliptical, and square, at the final time. An examination of the isothermal plates well depicts that the temperature experiences an uptrend from the NF pipes, and the plates laid on top of the pipes are hotter than the lower plates. Considering the isothermal plates, the minimum temperature arises around the pipes, and these plates are closer to the pipes on the fluid-inflow side rather than the outflowing side. In contrast, we can observe high-temperature plates on upper areas due to the radiation of the sun on the panel. The low-temperature isothermal plates twist inside the circular plates while stretching toward the lower wall of the PCM in elliptical and square pipes. In all pipe types, the low-temperature NF flows from the panel top and leads to these thermal variations in the PCM, especially when the temperature is maximal at various times. Circular pipes minimize the maximum temperature in the panel, while square and elliptical pipes

lead to equal maximum temperatures in the panel. The minimum temperature arising over the panel in the circular pipes is lowest in different shapes of the pipes.

Fig. 3 pictures the contour of the molten PCM in three vertical sections vs. four different times for three pipe shapes, i.e., circular, elliptical, and square. As observed, the temperature of PCM is high on the top of the pipe and low on the pipe sides. Therefore, the PCM melts on the top and solidifies at the bottom. Notably, the PCM is usually solid around the pipes and toward its lower layer while liquefying toward its upper layer. All pipe types include pin fins, which improve heat transmission between the PCM and the pipes. The pin fins are arranged uniformly all around the circular pipes and equally arranged on the top and down of the elliptical pipes. Likewise, two pin fins lie on every side of the square pipes to enable them to take the heat from the PCM better and transfer it to the NF. Temporal variations convert the solid PCM to liquid in different areas, especially in the lateral parts of the PCM layer. The volume of the liquid PCM is always larger on the upper layer of the PCM compared to other areas.

Fig. 4 displays the temperature contour on three vertical sections of the solar thermal panel and the underlying PCM vs. four different times for circular, elliptical, and square pipes. Thermal variations in the PCM layer stem from two parameters, i.e., solar radiation on the panel and the NF flowing in three pipe shapes. Solar radiation warms up the PCM layer from the top. On the other hand, the NF enters from one side and leaves from the other side while cooling the PCM. The area between the two pipes is the hottest space in the PCM layer at different times due to its distance from the pipes and NF and low heat transfer resulting from weak heat conduction in the PCM. The PCM temperature is lower in the

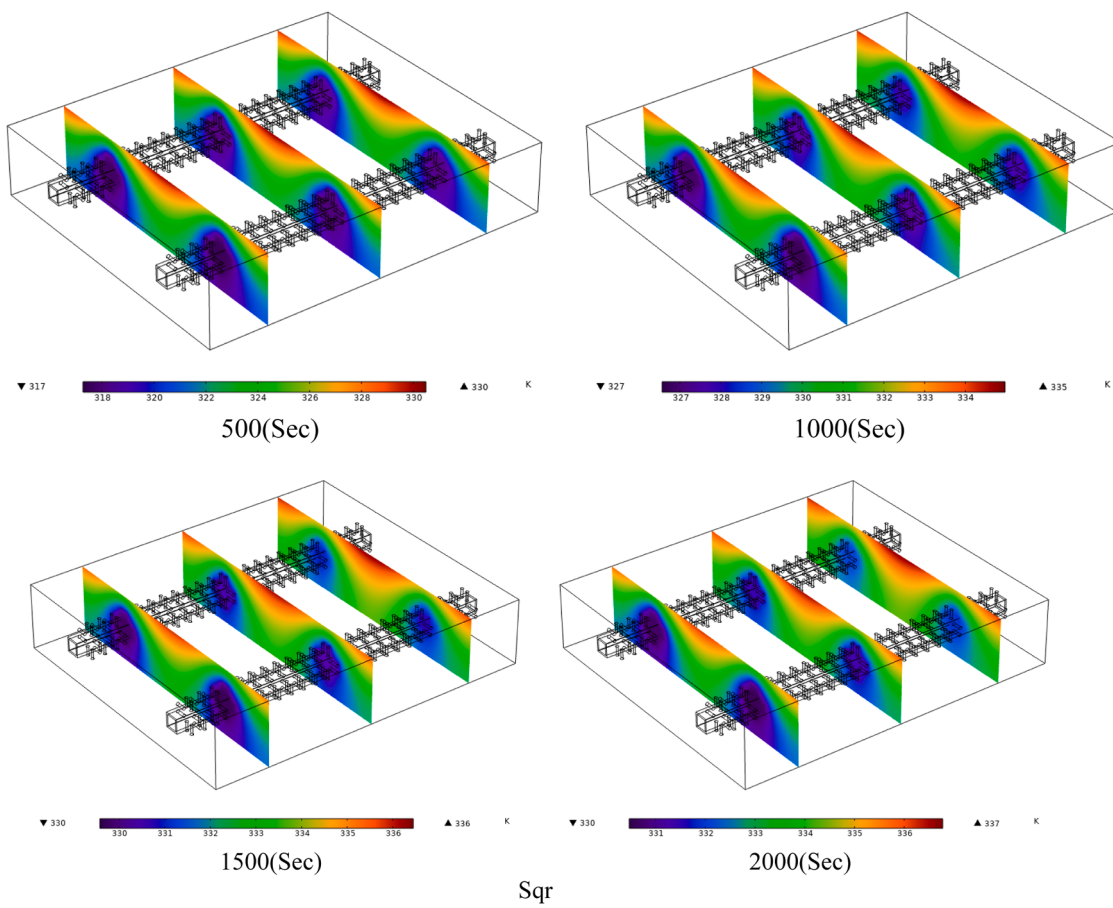


Fig. 4. (continued).

areas below and around the pipes due to their farness from the heat source and proximity to the pipes. The temperature is lower in the inlet section of the pipes than in other sections. The shape of the pipes has impacted the maximum and minimum temperatures at different times, and using one of the pipe shapes has lowered the maximum temperature at different times.

Fig. 5 depicts the thermal values of the output NF for circular, elliptical, and square pipe shapes when $t = 2000$ s. Any change in the pipe shape influences the contact area of the pipes with the PCM, as well as the profile of the NF in the pipe. Any changes to the pipe's velocity profile also impact the thermal and hydrodynamic boundary layers, as well as the temperature profile. The larger the contact area of the pipes with the PCM, the larger their heat transfer area. On the inner side, the contact area of the NF with the pipe augments and extends the heat transfer surface of the NF. From the beginning till the 500 s, the thermal change of the output NF experiences a sharp uptrend, and the change in the pipe shape slightly alters the temperature of the NF. However, after this time, the change in the pipe shape extensively shifts the thermal value of the NF. At this time, elliptical and circular pipes maximize and minimize the temperature of the output NF, respectively. The surface of the elliptical pipes creates the best contact area between the NF and PCM and improves heat transfer from the PCM to the NF. Thus, the NF is heated along the pipe, and its temperature rises at the outlet.

Fig. 6 shows the values of the heat transfer coefficient over circular, elliptical, and square pipe types when $t = 2000$ s. The explained heat transfer coefficient is estimated by averaging the local heat transfer coefficients. The variations in the area and the values of the local heat transfer coefficients influence the average heat transfer coefficient, and a change in the pipe shape impacts both of these factors. Thus, as observed, the pipe type extensively influences the average heat transfer

coefficient in the solar thermal panel and changes it from the outset to the end. The smallest heat transfer coefficient occurs in square pipes, and the mean heat transfer coefficient is maximal in circular pipes. When the time approaches the 2000s, the heat transfer coefficient becomes less variable, and the biggest differences among the heat transfer coefficients of the pipes with different shapes also arise. At this period, the heat transfer coefficient is 6.3 $\text{W/m}^2\text{K}$ larger in circular pipes than in elliptical pipes. Beside, the heat transfer coefficient is 12.7 $\text{W/m}^2\text{K}$ larger in elliptical pipes than in square pipes in the same period. Due to its symmetrical shape, the circular pipe can improve heat transfer, whose value is minimum in the corners of the other pipe types.

Fig. 7 illustrates the volume fraction of the molten PCM for three circular, elliptical, and square pipes when $t = 2000$ s. The solid-to-liquid conversion process of the PCM starts from its warmer areas and extends to other parts as the PCM gets hotter. At the beginning and end of the examined time, the solid PCM liquefies trivially. However, when the time reaches its middle, the solid PCM melts faster, and a considerable volume of it liquefies in a short period. Of course, any variation in the pipe shape slightly impacts the solid or liquid PCM when the time approaches 1000s, while after this time, the pipe type influences the volume of the solid or liquid PCM. The effect of the pipe type on the amount of the molten or solid PCM differs at different times. Elliptical pipes maximize the volume of the molten PCM at some times and the solid PCM at other times. In longer periods, it is observed that the circular pipes maximize the volume of the solid PCM, and the elliptical pipes increase the amount of the molten PCM. Both elliptical and circular pipes can alter the volume of the liquefied PCM by 5%. This difference in the liquefied PCM volume occurs when $t = 2000$ s.

Fig. 8 displays the average temperatures of the solar panel for three circular, elliptical, and square pipes when $t = 2000$ s. The change in the

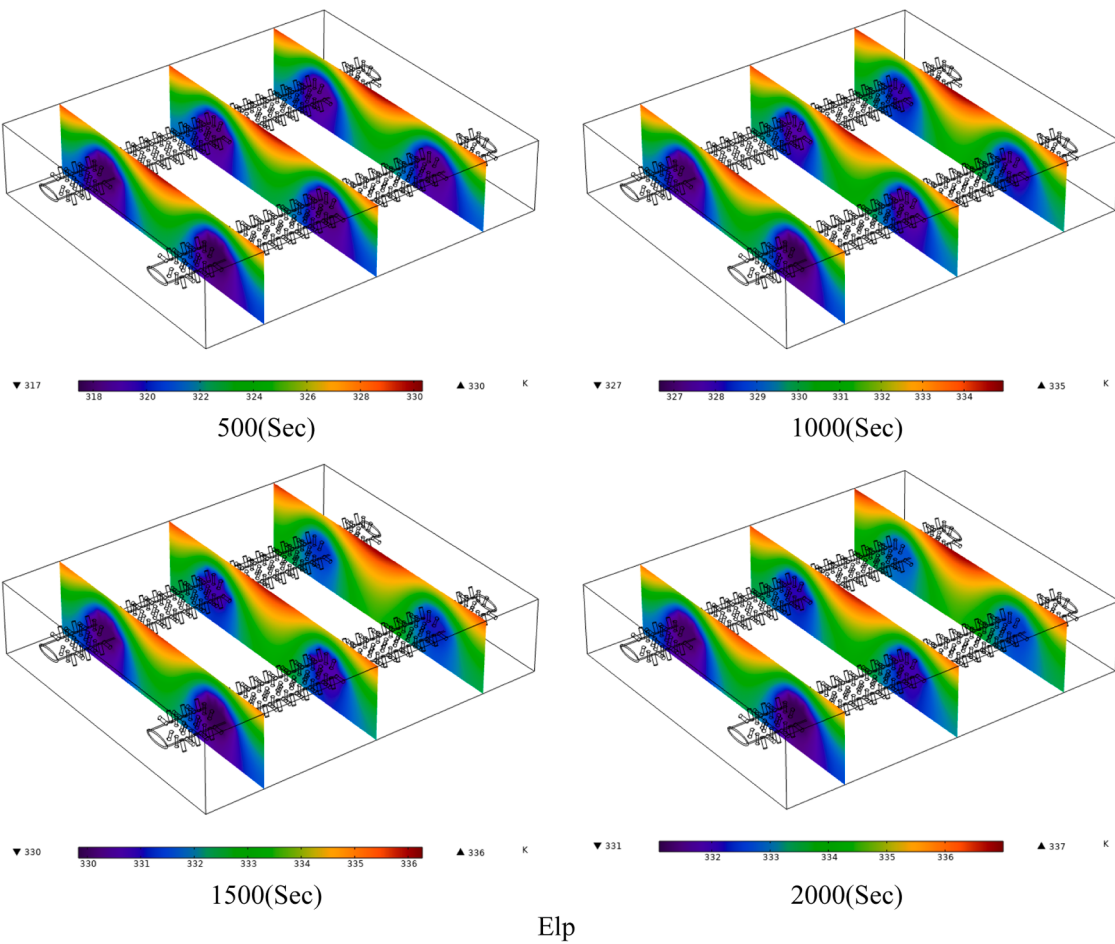
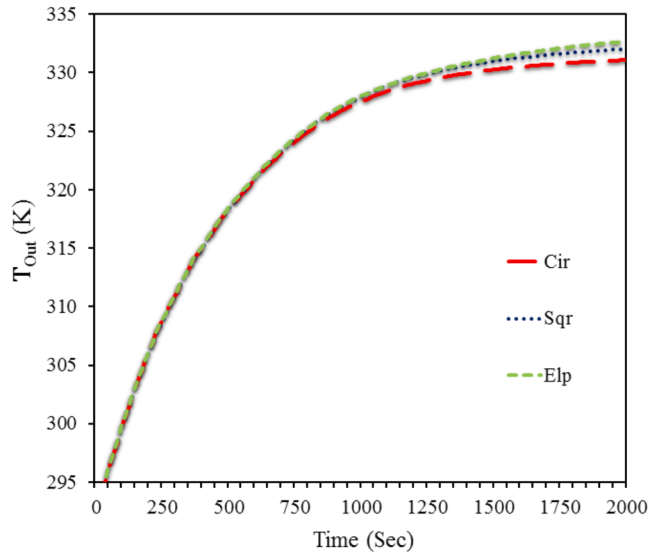
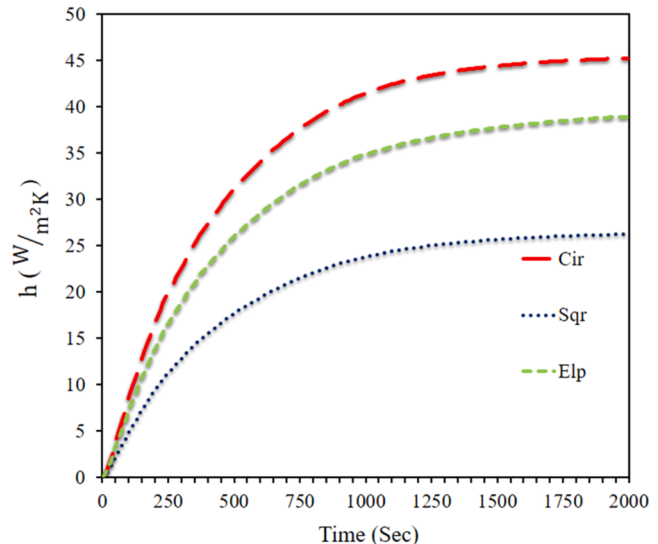


Fig. 4. (continued).

Fig. 5. The thermal values of the output NF for circular, elliptical, and square pipe shapes at $t = 2000$ s.

shape of the pipes used in the NF system below the solar thermal panel can alter the panel's temperature at various times, especially when the panel is hotter. Due to the heat of the sun, the panel's temperature goes up until it reaches a constant state. Elliptical pipes lower the temperature of the panel initially while maximizing the temperature over long

Fig. 6. The values of the heat transfer coefficient over circular, elliptical, and square pipe types at $t = 2000$ s.

periods. When $t > 1000$ s, the circular pipes give rise to the lowest temperature on the panel. The contact area between the NF and PCM is significant, and its alteration influences the amount of heat the NF generally receives from the PCM. The rate of heat transfer from the sharp corners of elliptical and square pipes is trivial due to the lower flow of

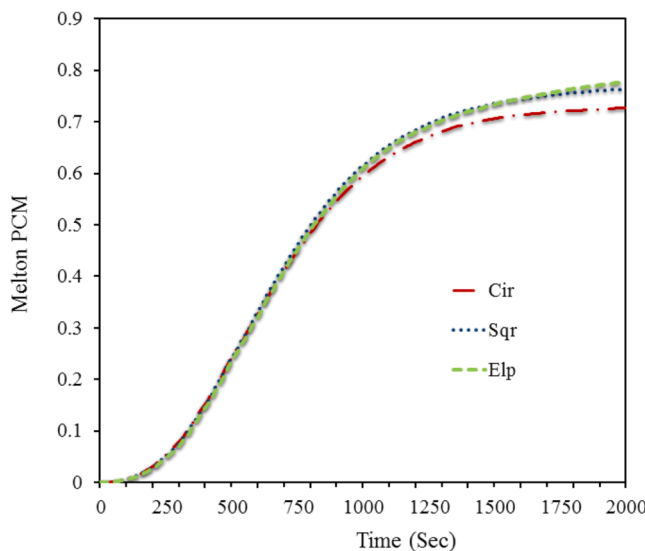


Fig. 7. The volume fraction of the molten PCM for three circular, elliptical, and square pipes at $t = 2000$ s.

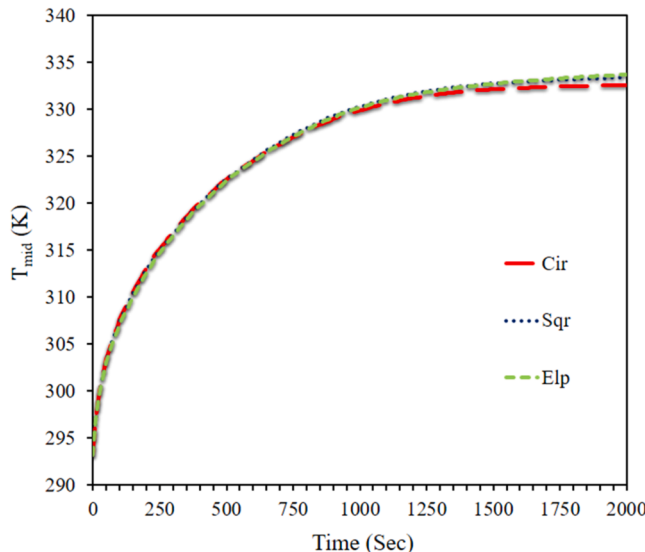


Fig. 8. The average temperatures of the solar panel for three circular, elliptical, and square pipes at $t = 2000$ s.

the NF. Owing to its symmetricity, the circular pipe improves the flow of the NF in the pipe and usually reduces the panel's temperature to a large degree. The square pipes manifest a behavior between the circular and elliptical pipes and lead to a panel temperature between these two pipe types. A change in the pipe shape can alter the panel temperature by $>1^\circ$, such that circular pipes reduce the panel temperature by 1.13 more than the elliptical pipes at the final time.

5. Conclusion

This study transiently analyzed the effect of applying different shapes of NF-conveying pipes on a thermal solar panel system. Two pipes with circular, elliptical, and square shapes were employed in this system, and spherical pin fins were installed over the pipes lying inside the PCM. The water NF and silver nanoparticles were used in the pipes. The results showed that:

- 1 Elliptical pipes minimize the panel temperature when $t < 1000$ s and maximize the temperature on the pipes after this period.
- 2 When $t = 2000$ s, circular pipes can reduce the panel temperature by $>1^\circ$ compared to the elliptical pipes.
- 3 Circular pipes maximize the volume of the solid PCM, and elliptical pipes increase the amount of the molten PCM. The biggest difference in the volume of the liquefied PCM is 5% when $t = 2000$ s.
- 4 When $t = 2000$ s, the heat transfer coefficient is 16.17% larger in circular pipes than in elliptical pipes, and the heat transfer coefficient is 48.43% higher in elliptical pipes than in square pipes.
- 5 A change in the pipe shape trivially impacts the NF's temperature at the outlet until the time reaches 500 s. However, elliptical pipes maximize the temperature of the output NF at longer periods, while circular pipes minimize the NF's temperature at the outlet.

Declaration of Competing Interest

The authors declare that they have no known competing financial interests or personal relationships that could have appeared to influence the work reported in this paper.

Data availability

Data will be made available on request.

References

- [1] Izadi M, El Haj Assad M. Chapter 15 - Use of nanofluids in solar energy systems. In: Assad MEH, Rosen MA, editors. Design and performance optimization of renewable energy systems. Academic Press; 2021. p. 221–50.
- [2] Wang G, Yin J. Design and exergy evaluation of a novel parabolic trough solar-nuclear combined system. Ann Nucl Energy 2020;144:107573.
- [3] Nasraoui H, Driss Z, Kchaou H. Novel collector design for enhancing the performance of solar chimney power plant. Renew Energy 2020;145:1658–71.
- [4] Shojaeizadeh E, Veysi F, Goudarzi K. Heat transfer and thermal efficiency of a lab-fabricated ferrofluid-based single-ended tube solar collector under the effect of magnetic field: an experimental study. Appl Therm Eng 2020;164:114510.
- [5] Yerdesk Y, Abdulina Z, Aliuly A, Belyayev Y, Mohanraj M, Kaltayev A. Numerical simulation on solar collector and cascade heat pump combi water heating systems in Kazakhstan climates. Renew Energy 2020;145:1222–34.
- [6] Khanlari A, Güler HÖ, Tuncer AD, Şirin C, Bilge YC, Yılmaz Y, Güngör A. Experimental and numerical study of the effect of integrating plus-shaped perforated baffles to solar air collector in drying application. Renew Energy 2020; 145:1677–92.
- [7] Farhadi R, Taki M. The energy gain reduction due to shadow inside a flat-plate solar collector. Renew Energy 2020;147:730–40.
- [8] Mahon D, Henshall P, Claudio G, Eames PC. Feasibility study of MgSO₄ + zeolite based composite thermochemical energy stores charged by vacuum flat plate solar thermal collectors for seasonal thermal energy storage. Renew Energy 2020;145: 1799–807.
- [9] Choudhary S, Sachdeva A, Kumar P. Investigation of the stability of MgO nanofluid and its effect on the thermal performance of flat plate solar collector. Renew Energy 2020;147:1801–14.
- [10] Anirudh K, Dhinakaran S. Performance improvement of a flat-plate solar collector by inserting intermittent porous blocks. Renew Energy 2020;145:428–41.
- [11] Saffarian MR, Moravej M, Doraneghard MH. Heat transfer enhancement in a flat plate solar collector with different flow path shapes using nanofluid. Renew Energy 2020;146:2316–29.
- [12] Aljaeraani HA, Samykano M, Pandey AK, Kadrigama K, Saidur R. Thermo-physical properties and corrosivity improvement of molten salts by use of nanoparticles for concentrated solar power applications: a critical review. J Mol Liq 2020;314: 113807.
- [13] Salisu S, Mustafa MW, Olatomiwa L, Mohammed OO. Assessment of technical and economic feasibility for a hybrid PV-wind-diesel-battery energy system in a remote community of north central Nigeria. Alex Eng J 2019;58:1103–18.
- [14] Jiang Z, Palacios A, Lei X, Navarro ME, Qiao G, Mura E, Xu G, Ding Y. Novel key parameter for eutectic nitrates based nanofluids selection for concentrating solar power (CSP) systems. Appl Energy 2019;235:529–42.
- [15] Sharma P, Naidu RChinnappa. Optimization techniques for grid-connected PV with retired EV batteries in centralized charging station with challenges and future possibilities: a review. Ain Shams Eng J 2023;14:101985.
- [16] Roper R, Harkema M, Sabherwall P, Riddle C, Chisholm B, Day B, Marotta P. Molten salt for advanced energy applications: a review. Ann Nucl Energy 2022; 169:108924.

- [17] Salilah EM, Abu-Hamdeh NH. Charging process of thermal energy storage system under varying incident heat flux: interaction the fluid neighbour nodes and particles in order to heat transfer. *J Therm Anal Calorim* 2021.
- [18] Ebrahimpour Z, Sheikholeslami M. Investigation of nanofluid convective flow through a solar system equipped with mirrors. *J Mol Liq* 2021;335:116198.
- [19] Alizadeh H, Ghasempour R, Shafii MB, Ahmadi MH, Yan WM, Nazari MA. Numerical simulation of PV cooling by using single turn pulsating heat pipe. *Int J Heat Mass Transf* 2018;127:203–8.
- [20] Raj P, Subudhi S. A review of studies using nanofluids in flat-plate and direct absorption solar collectors. *Renew Sustain Energy Rev* 2018;84:54–74.
- [21] Krauter S. Increased electrical yield via water flow over the front of photovoltaic panels. *Sol Energy Mater Sol Cells* 2004;82:131–7.
- [22] Hartmann N, Glueck C, Schmidt FP. Solar cooling for small office buildings: comparison of solar thermal and photovoltaic options for two different European climates. *Renew Energy* 2011;36:1329–38.
- [23] Kim DJ, Kim DH, Bhattacharai S, Oh JH. Simulation and Model Validation of the Surface Cooling System for Improving the Power of a Photovoltaic Module. *J Sol Energy Eng* 2011;133.
- [24] Prudhvi P, Sai PC. Efficiency improvement of solar PV panels using active cooling. In: Proceedings of the 2012 11th International Conference on Environment and Electrical Engineering; 2012. p. 1093–7.
- [25] Teo HG, Lee PS, Hawlader MNA. An active cooling system for photovoltaic modules. *Appl Energy* 2012;90:309–15.
- [26] Habiballahi M, Ameri M, Mansouri SH. Efficiency improvement of photovoltaic water pumping systems by means of water flow beneath photovoltaic cells surface. *J Sol Energy Eng* 2015;137.
- [27] Tripanagnostopoulos Y, Nousia T, Souliotis M, Yianoulis P. Hybrid photovoltaic/thermal solar systems. *Sol Energy* 2002;72:217–34.
- [28] Zyta G, Fal J. Viscosity, thermal and electrical conductivity of silicon dioxide–ethylene glycol transparent nanofluids: an experimental studies. *Thermochim Acta* 2017;650:106–13.
- [29] Li M. A nano-graphite/paraffin phase change material with high thermal conductivity. *Appl Energy* 2013;106:25–30.
- [30] M. Ishii, Thermo-fluid dynamic theory of two-phase flow, J NASA Sti/recon Technical Report A, 75 (1975) 29657.
- [31] M. Manninen, V. Taivassalo, S. Kallio, On the mixture model for multiphase flow, (1996).
- [32] Schiller L. A drag coefficient correlation. *J Zeit. Ver. Deutsch. Ing.* 1933;77: 318–20.
- [33] R. Nasrin, M. Hasanuzzaman, N.A. Rahim, Effect of high irradiation on photovoltaic power and energy, 42 (2018) 1115–31.
- [34] Rahman MM, Hasanuzzaman M, Rahim NA. Effects of operational conditions on the energy efficiency of photovoltaic modules operating in Malaysia. *J Clean Prod* 2017;143:912–24.